Journal of the Mechanical Behavior of Biomedical Materials 168 (2025) 107006

Contents lists available at ScienceDirect

Journal of the Mechanical Behavior of Biomedical Materials

journal homepage: www.elsevier.com/locate/jmbbm

3D-printed programmable bistable mechanisms for customized wearable devices in tremor attenuation

Moslem Mohammadi [a], Abbas Z. Kouzani [a], Mahdi Bodaghi [b], Ali Zolfagharian [a,*]

[a] School of Engineering, Deakin University, Geelong, Victoria 3216, Australia
[b] Department of Engineering, School of Science and Technology, Nottingham Trent University, Nottingham NG11 8NS, UK

A R T I C L E I N F O

Keywords:
Compliant mechanism
Tremor
Vibration
Wearable devices
metamaterials
3D/4D printing

A B S T R A C T

This research proposes a computational framework for designing a compliant bistable mechanism and fabricating it using 3D printing for customized medical applications. The proposed method reduces upper limb tremors, taking advantage of the nonlinear mechanical properties of flexible structures. The model's development and execution on a single platform streamlines integrated inverse design and simulation, simplifying the customization process. A synthetic human arm model, built to imitate a human wrist, was scanned with a light detection and ranging (LiDAR) sensor to customize the 3D model of the bistable structure. Afterwards, the arm model was used to test the bistable mechanism. Automating the inverse design process with a deep neural network (DNN) and evolutionary optimization decides the optimal bistable mechanism configurations for stiffness and vibration attenuation. The pseudo-rigid-body model (PRBM) of the bistable mechanism was developed to train the machine learning (ML) model in the inverse design, making it computationally affordable to find the optimal parameters of bistable structure for a specific mechanical response based on tremor characteristics. Experimental results showing up to 87.11 % reduction in tremor power while weighing only 27 g to reduce vibrations in various situations suggest its use in 4D printing of wearable orthotic devices for Parkinsonian tremors and related diseases.

1. Introduction

Involuntary, rhythmic movements, or tremors, can have a major negative influence on a person's quality of life, especially for those who suffer from Parkinson's disease (PD) or essential tremors (ET) (Marsden et al., 1984; Puschmann and Wszolek, 2011; Mohammadi et al., 2022). Even though current therapies, including drugs and surgery, provide comfort (Sasso et al., 1990; Shanker, 2019; Cury et al., 2017), they are not always successful and frequently have negative side effects (Armstrong and Okun, 2020; Baizabal-Carvallo et al., 2014). Wearable technology and robotic exoskeletons are two non-invasive options that have recently shown promise in controlling tremors without requiring surgery (Masoumi, 2018; Rudraraju and Nguyen, 2018a; Zahedi et al., 2021; Herrnstadt and Menon, 2013; Herrnstadt et al., 2019/02; Skaramagkas et al., 2021). These solutions, however, have issues with comfort, usability, and real-time adaptation to the dynamic nature of tremors (Mohammadi et al., 2022). Although they might offer stability, the traditional stiff structures used in these devices are unable to adapt to the variations in tremor frequency and intensity (Nazari et al., 2023; Bao et al., 2019). This drawback emphasizes the need for more adaptable solutions, ones that can modify their mechanical characteristics in response to the intensity of tremors, resulting in customized and successful control techniques (Voloshina, 2024; Mohammadi et al., 2023).

Compliant mechanisms, which exploit the bending of flexible beams rather than traditional rigid joints, have drawn more interest in engineering studies (Howell, 2013; Gomez et al., 2017). Compliant actuators (Ling et al., 2022), robot joints (Mohammadi et al., 2024), grippers (Hao et al., 2018; McGowan and Hao, 2023), aerospace field (Zhang et al., 2024), continuum robots (Li and Hao, 2021), and morphing wings (Achleitner et al., 2019) are just a few of the many applications for these mechanics. The ability of bistable systems to sustain two states of stability requiring constant power gives them specifications to be very useful in a range of applications, including micro-electromechanical systems (MEMS) (Masters and Howell, 2003; Huang and Yang, 2012), mechanical metamaterials (Yang and Ma, 2019, 2020; Chen et al., 2023), energy harvesting (Wu and Xu, 2022), rapid mechanical transitions (Radisson and Kanso, 2023) and morphing and deployable structures (Liu and Hao, 2022; Librandi et al., 2020). This paper examines the

* Corresponding author.
E-mail address: a.zolfagharian@deakin.edu.au (A. Zolfagharian).

https://doi.org/10.1016/j.jmbbm.2025.107006
Received 8 January 2025; Received in revised form 30 March 2025; Accepted 10 April 2025
Available online 17 April 2025

design and application of a compliant bistable mechanism with unique stiffness characteristics that make it ideal for controlling tremors.

The inverse design of flexible structures has seen significant advancements with the application of machine learning (ML) (Liu et al., 2020; Deng et al., 2022; Zhang et al., 2025) and optimization algorithms (Kumar et al., 2020; Liu et al., 2023; Zheng et al., 2023). Methods for designing such structures involve complex simulations like finite element analysis (FEA) (Oladipo et al., 2023) or reduced-order modelling (ROM) (Wang and Amirkhizi, 2023), which can be time-consuming and computationally intensive. To overcome these limitations, researchers have employed ML techniques that allow for faster and more accurate design optimization. For instance, recent studies have successfully utilized neural networks, trained on topology-optimized datasets, to predict desired mechanical responses of flexible structures efficiently (Li et al., 2023; Rastegarzadeh et al., 2023). Advanced models, such as deep neural networks (DNN) combined with optimization algorithms like particle swarm optimization and genetic algorithms (GA) (Zheng et al., 2023; Zeng et al., 2023), facilitate the rapid prediction and fine-tuning of parameters, reducing the iteration costs associated with experimental methods. In particular, DNNs have been applied to designing nonlinear responses, such as the buckling and snapping behaviours in bistable structures (Bazmara et al., 2023). This approach streamlines the process by integrating the predictive power of neural networks with automated optimization techniques, creating a more efficient pathway for achieving desired mechanical properties in flexible, vibration-damping structures. Even though the inverse design of the structure has benefits, modelling bistable mechanisms in this research is essential for collecting training data for DNN and evaluating the optimization results.

Accurate modelling is challenging as these mechanisms often involve significant shape changing, such as in beams that undergo large deflections (Liu et al., 2024). Simplified, computationally efficient models are crucial in this context, allowing for effective analysis of force-displacement relationships, deformation profiles, strain energy, and stress without the extensive computational costs associated with methods such as FEA (Bilancia and Berselli, 2021). Even though a number of techniques have been developed to solve these issues, such as the elliptic integral solution (EIS) (Holst et al., 2011), beam constraint model (BCM) (Sen and Awtar, 2013), and smooth curvature model (SCM) (Odhner and Dollar, 2012), each has drawbacks when used on complex bistable processes. The pseudo-rigid-body model (PRBM) offers an advantageous approach for this task, using rigid-body components with equivalent force-deflection characteristics to predict deflections accurately (Yu and Zhu, 2017; Jin et al., 2020). Variants of the PRBM (nR-PRBM with n revolute joints and n+1 rigid links) address different levels of accuracy and complexity. While the 1R-PRBM provides a simplified model, it is less accurate at high deflection angles, leading to the development of the 4R-PRBM for the structure in this study due to increased accuracy and efficiency meanwhile keeping the computational requirements low, relatively. The 4R-PRBM model of the flexible links is modelled in MATLAB/Simulink to measure the structures' static and dynamic properties.

This work proposes a compliant bistable mechanism to fill a major gap in the design of a mechanically adaptive orthotic mechanism for tremor reduction, specifically for patients with PD and ET (Mohammadi et al., 2022). Conventional orthotic designs are inflexible, which can make daily tasks difficult, and lack the flexibility to offer both strong tremor resistance and ease of voluntary movement. The main contribution of this study is the inverse design and simulation of the bistable mechanism in a single environment with minimal computational cost and time. Additionally, a vibration-attenuating mechanism that is bistable and can transition between stable states with low energy costs has been experimentally validated, making it viable for real-world applications. Furthermore, the incorporation of DNN models trained on the simulated dataset enables the mechanism's rapid inverse development, which, through parameter optimization, makes it adjustable to various user requirements.

The paper is structured as follows. In Section 2, the proposed compliant bistable mechanism is modelled. The 4R-PRBM and the Simscape simulation setup are used to test the structure's vibration-damping properties, and the integration of DNN models with a GA is highlighted as an effective inverse design for achieving desired mechanical responses. In Section 3, experimental validation and performance comparisons between simulated and constructed models are examined, as well as the structure's tremor attenuation capabilities and possible wearable use. Section 4 concludes with a summary of the results, implications for applications including tremor mitigation, and suggestions for a further study on improving flexible, adjustable orthotic devices.

2. Methodology

The proposed mechanism's main characteristic in this research, shown in Fig. 1, is its bistable nature, in which each unit has negative stiffness throughout the transition between stable states but very high stiffness at the start of moving in each stable state (stiffness curves are depicted in Fig. 2b). By offering strong resistance at the stable states, this characteristic allows the mechanism to withstand small involuntary tremor-induced displacements. However, if the applied force is greater than a threshold (the maximum force in the stiffness curve), the negative stiffness during the transition facilitates controlled and smooth movement between the two stable states. Because of its flexibility in high forces and strong resistance for minor displacement, the mechanism can adjust to external forces and vibrations of various frequencies and intensities. Fig. 1a shows the proposed structure on the human hand to control the flexion/extension tremor. Fig. 1b shows the proposed wearable mechanism consists of five bistable units. As shown in Fig. 1, the voluntary motion in the wrist needs 20 mm stretching, on average, in the orthosis, which requires a 4 mm stroke from one stable state to the other for each bistable unit, on average.

For clarification, a hypothetical example is shown in Fig. 2b. The features of the tremor in Fig. 2b has a force maximum of ± 10 N (indicated by red dashed lines). Also, the voluntary displacement (amplitude of the voluntary motion signal) in this scenario is assumed to be 30 mm which needs each unit 6 mm stroke. The tremor displacement amplitude before installing the orthosis is 5 mm (equal to 1 mm across any of the five units). The design purpose in this example is to reach 80 % attenuation which is equal to achieving a 0.2 mm amplitude per unit (vertical blue dashed lines). The desired stiffness curve (solid blue line) in Fig. 2b ensures the transition force is about twice the tremor force for safety, limiting tremor displacement to 0.15 mm per unit to avoid exceeding design constraints. This target stiffness is input into our inverse design process to derive the desired unit geometry.

2.1. Mathematical model

In this study, we use the PRBM model to simulate the mechanism design, which quantifies a flexible link into a sequence of solid bricks joined by revolute joints. The flexible joints between the solid bricks mimic the elasticity of a continuous structure, while each solid brick serves as a firm link. Although this leads to increased computational complexity and longer simulation periods, we enhance the approximation of a flexible link by increasing the number of solid links and revolute joints. As a result, 4R-PRBM was used to balance simulation time and accuracy as per the preliminary study (Fig. 2a). The cross-sectional shape, length, and material of the flexible body all affect the stiffness of the flexible links, which is estimated by the stiffness of the revolute joints. Additionally, a dimensionless stiffness coefficient called α is used to scale the torsional stiffness of the revolute joints to approximate the bending stiffness of the flexible link (i.e. $K_d = \alpha\frac{EI}{l}$, where K_d is the stiffness of a joint). The geometric configuration determines the value of

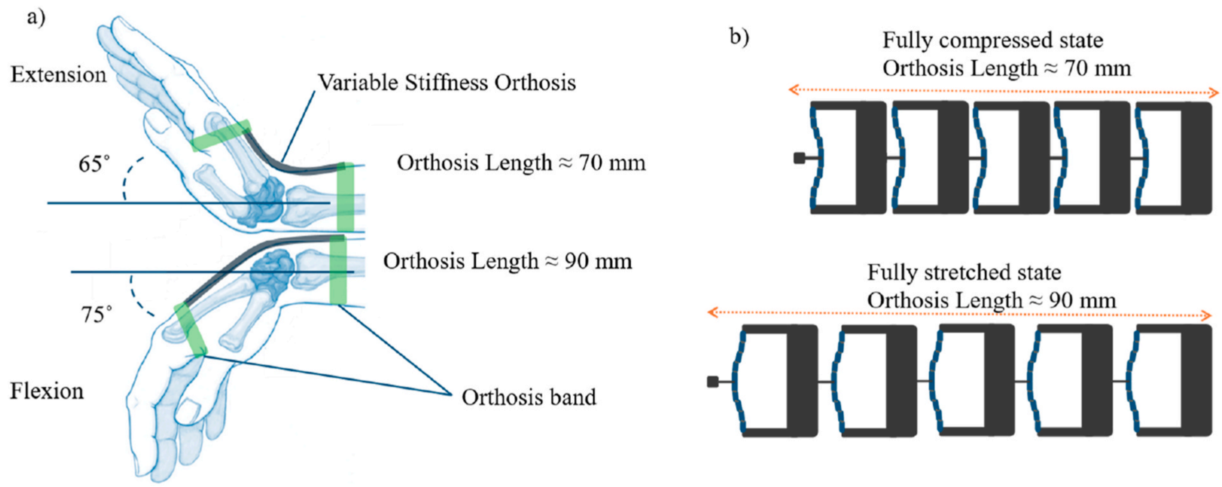

Fig. 1. Hand orthosis with five compliant bistable units. a) Compliant orthosis mounted on the hand in full range movement of wrist extension/flexion motion. b) Compliant orthosis includes five compliant bistable unit in fully compressed (up) and fully stretched state (down).

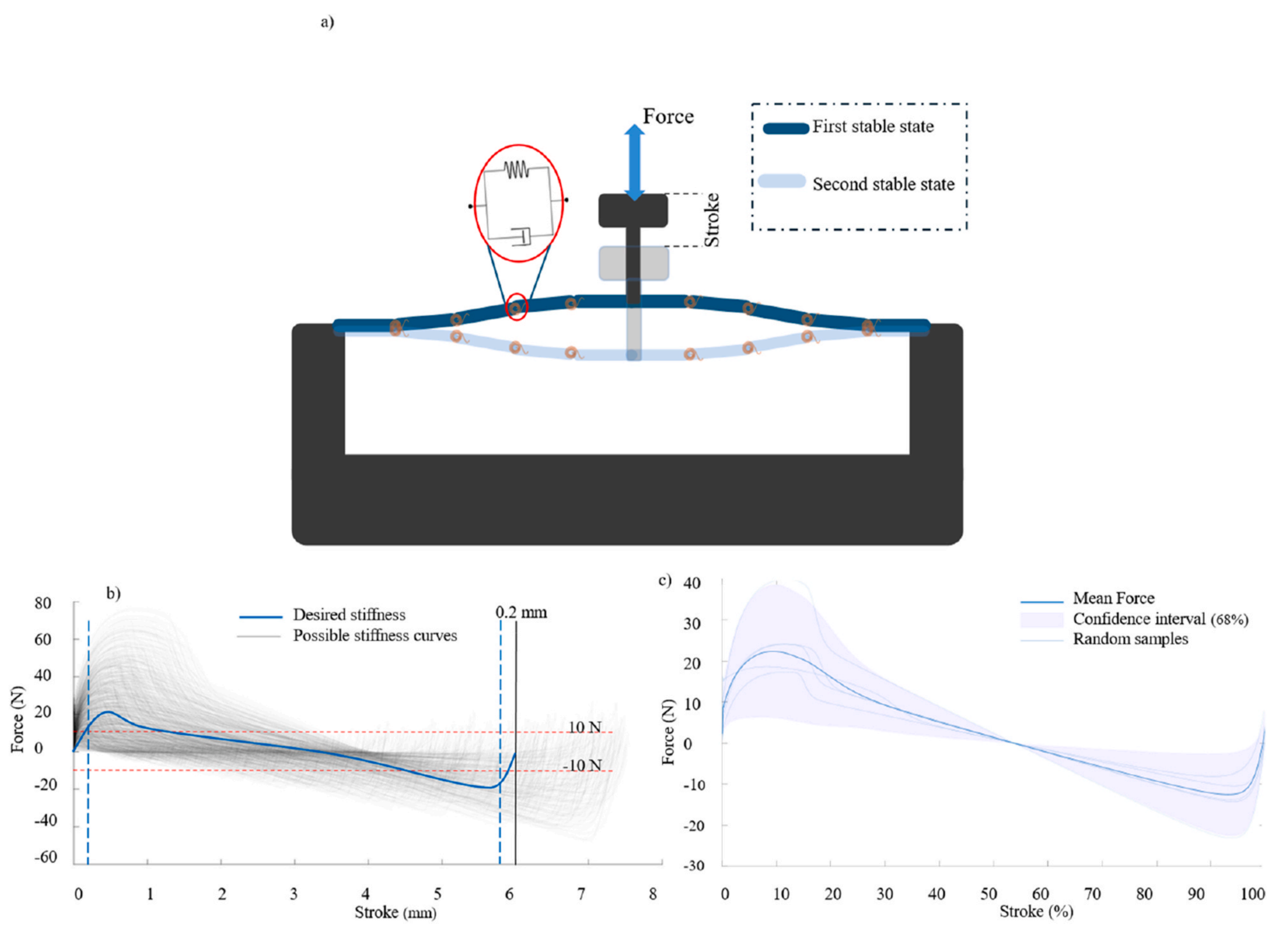

Fig. 2. a) PRBM model of the bistable structure in two stable states. b) Force-stroke curves of the 1000 simulation. A hypothetical example of a stiffness curve with stroke of 6 mm desired to stop tremor with maximum 10N force. c) Average and the confidence intervals of the force-stroke curves of the simulation results.

α, which is based on empirical evidence. Despite the fact that MATLAB/Simscape offers a flexible body, the PRBM model was chosen for this investigation because of its processing costs (Yu et al., 2005).

The kinetic energy T and potential energy U contained in the model are determined using the PRBM by:

$$U = \sum_i \frac{1}{2} K_{d,i} \theta_i^2 \tag{1}$$

$$T = \sum_i \frac{1}{2} J_i \dot{\theta}_i^2 \tag{2}$$

where θ_i is the angle of rotation for the i_th joint. J_i and $K_{d,i}$ represent the rotational inertia (moment of inertia) of the rigid segment and torsional stiffness associated with the i-th joint. Using Lagrange's equation for each generalized coordinate θ_i:

$$\frac{d}{dt}\left(\frac{\partial L}{\partial \dot{\theta}_i}\right) - \frac{\partial L}{\partial \theta_i} = Q_i \tag{3}$$

where Q_i is the generalized force associated with θ_i (e.g., due to external forces or moments acting on the segment). As a result, the following set of corresponding differential equations is produced:

$$J_i \ddot{\theta}_i + K_{d,i}\theta_i = Q_i \tag{4}$$

The following is a definition of a state-space model for this system:

$$x_i = \begin{bmatrix} x_{i1} \\ x_{i2} \end{bmatrix} = \begin{bmatrix} \theta_i \\ \dot{\theta}_i \end{bmatrix} \tag{5}$$

$$\dot{X} = AX + BU \tag{6}$$

Where A is a matrix with each block given by $\begin{bmatrix} 0 & 1 \\ \frac{k_{d,i}}{J_i} & 0 \end{bmatrix} x_i$, B is a vector where each entry is $\begin{bmatrix} 0 \\ \frac{1}{J_i} \end{bmatrix}$, and U is the input vector which is the applied forces or torques at each joint (Yu et al., 2005). The supplemental material explains the detailed model.

2.2. Simulations

The mechanical behaviour of a human wrist joint and hand was simulated as a 0.45 kg mass attached to the ground with a joint that has a stiffness and damping effect similar to an adult's wrist characteristics. Since the stiffness and damping of the arm can vary under different conditions, this study assumes an average constant value to simplify the model, selected based on findings from the literature review (Milner and Cloutier, 1998). Damping of the wrist joint during voluntary movement A flexible, bistable mechanism is attached between the 0.45 kg mass (represents the hand), and the ground (which represents the forearm). The structure is depicted in the supplementary document, Fig. S1. This bistable mechanism acts as an orthosis, designed to attenuate vibration. Also in the simulation, the energy needed to move the hand which is moving the structure from one stable state to another, is depicted in Fig. 2, is evaluated as a necessary action during voluntary motion in real-life scenarios where a subject may move their hand apart from the tremor motion. Fig. 2a shows the 4R-PRBM of the bistable mechanism. Each flexible link is modelled as five rigid bodies and 4 revolute joints. Each joint has its own stiffness and damping effect which are chosen in the mentioned method in the mathematic model section based on $K_d = \alpha \frac{EI}{l}$, where E was obtained based on the ASTM D638-14 standard that shows Young's modulus equal to 2300 MPa and α is empirically calibrated through an iterative process.

The simulation was run 1000 times, where each iteration involved testing the stiffness characteristics of the bistable structure under randomized configurations. Each trial applied a 5 Hz sinusoidal force, a frequency commonly associated with tremors in patients with PD, to the model. To evaluate various properties and structural configurations, the joints' stiffness and damping values, and the initial angle of the joints (which adjust the curvature in the initial shape of the flexible link) were randomized within feasible ranges. Selecting the right material is crucial for component performance because it directly influences bistability. For compliant mechanisms, a high strength-to-modulus ratio is ideal since it allows for greater deflection before failure. Researchers demonstrated that acrylonitrile butadiene styrene (ABS) can be used to fabricate a bistable mechanism prototype that performs efficiently, while also offering easier fabrication (Zolfagharian et al., 2025; Zirbel et al., 2016). In this research, ABS has been chosen as the material for the bistable component.

During each simulation, the structures' transition between stable states is executed at a constant velocity to collect the required force and then calculate the stiffness curve. During this test, the structure undergoes snap-through, moving the mechanism from one stable state to the other. Analysing the resultant stiffness curve allows for calculating the energy required to transition the structure between these stable states. This energy, computed as the integral of the force-displacement curve over regions where positive force is applied, is particularly relevant for determining the orthosis's usability. The required energy level indicates whether the structure comfortably allows human voluntary motion while attenuating the tremor in the wrist and forearm. If the energy demand is excessively high, the structure may resist movement, rendering it impractical for patients, as it could prevent voluntary motion of the hand. Furthermore, the full displacement between two stable states is calculated from the stiffness curve.

In addition to analysing the energy requirement, the vibration attenuation capabilities of each configuration were evaluated. By comparing the vibration attenuation in each simulated configuration to a baseline condition (with the force applied directly to the wrist joint and hand model alone without the bistable structure in between), the simulation assesses how well different configurations dampen tremors. This comparison provides insights into which configurations may be optimal for practical application in reducing tremor intensity in PD patients. The simulation results are displayed in Figs. 2 and 3.

Fig. 2b presents the stiffness curve, showing the bistable behaviour as the structure moves between stable states under applied force and Fig. 2c shows the average stiffness curve with its confidence interval. Fig. 3a and Fig. 3b are scatter plots illustrating the relationship between the tremor attenuation and energy required to transition states versus the stiffness of the joints and angle of the links for each configuration respectively. As is shown in the figures, the tremor attenuation in all various configurations is significantly effective. On the other hand, when the joint stiffness and angle increase, the transition required energy increases as well and becomes relatively high (for some configurations reaches 150 J) for some of the configurations that making it not feasible to use as a tremor mitigator in the human upper arm (the subject will not be able to move at all).

Finally, Fig. 3c depicts the maximum force each configuration can achieve, plotted against the link angles and joint stiffness to highlight the dependence on joint configuration. Maximum required force, like transition required energy, is a parameter to evaluate whether the compliant mechanism allows voluntary motion in upper limbs or not. These results allow for a detailed assessment of each configuration's energy efficiency, vibrational damping, and overall flexibility, contributing to the understanding of which structure designs might offer the best combination of tremor attenuation and ease of use in an orthotic application.

2.3. DNN

The dataset generated from the Simscape simulation, which included 1000 samples of the compliant mechanism exhibiting snap-through behaviour, was utilized to train Deep Neural Network (DNN) models. The goal was to enable the DNNs to learn and predict various mechanical properties of the structure, including the required energy for transition, maximum required force, tremor attenuation performance, and stiffness curves. The approach was designed to capture the nonlinear relationships between mechanical parameters and their responses under varying configurations. Before training the DNNs, the dataset underwent preprocessing. The parametric data encompassed features such as joint angle and material properties (i.e., length, cross-section, and Young's modulus which is applied in joint stiffness for simulation). Each feature was normalized to ensure consistency, thereby facilitating network

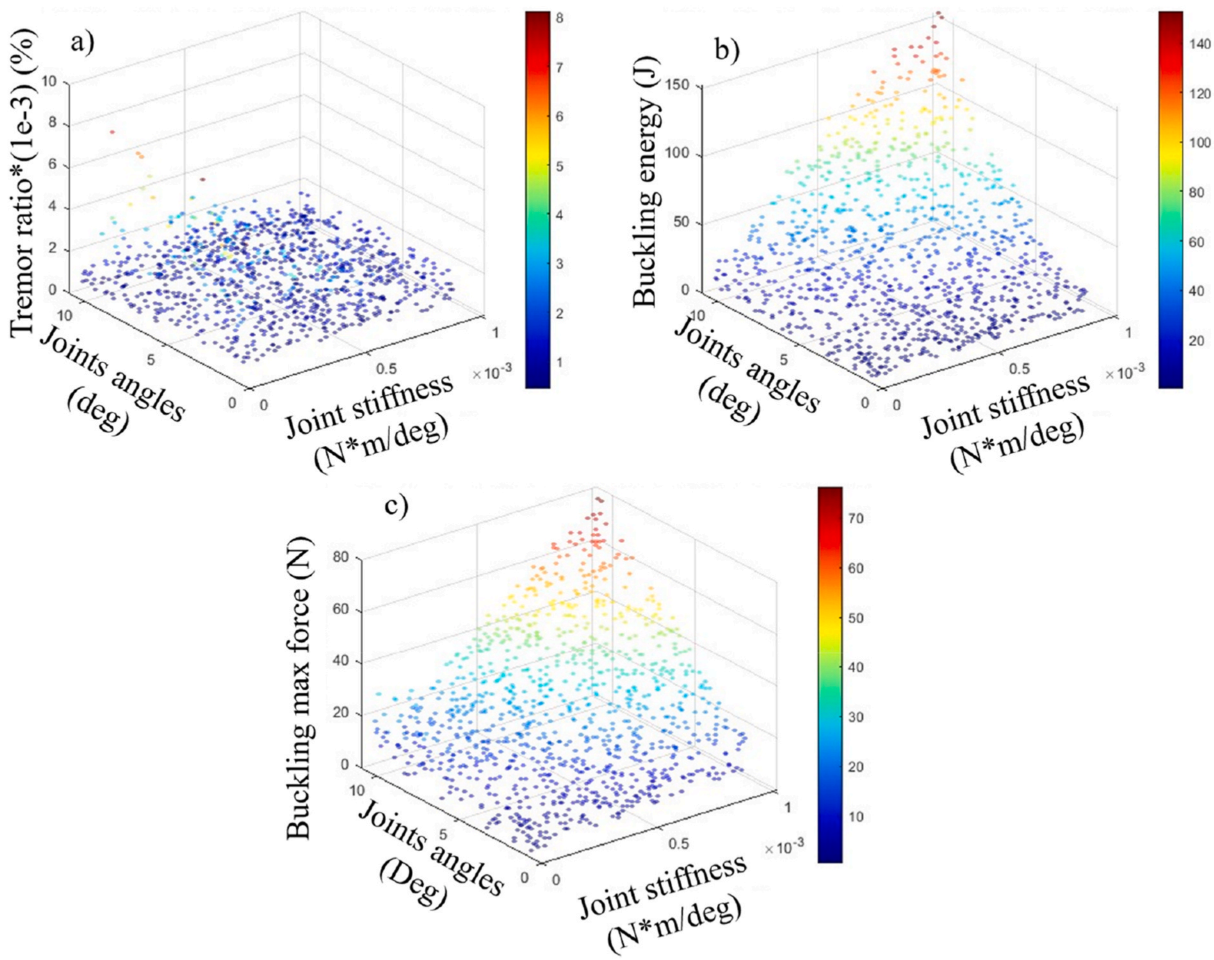

Fig. 3. a) Scatter plot of the vibration amplitude ratio(*1e-3 %), compared to reference signal with no compliant mechanism. b) Scatter plot of the required energy for transition between the first stable state to the second state. c) Scatter plot of the maximum required force in the stiffness curve.

convergence and generalization.

The architecture of the DNN models was designed to be robust, with multiple fully connected layers to accommodate complex learning. Each network was configured with an input layer reflecting the dimensional space of the dataset features, followed by dense layers with ReLU activation to capture the nonlinearities presented in mechanical responses. Two DNN models were utilized in this paper to predict various properties of the structures. The simpler model for predicting parameters including energy for one stroke, maximum required force to stroke, and stroke displacement has a hidden layer with 32 neurons and two additional layers with 64 neurons, balancing learning capacity with computational efficiency. The output layer was designed to predict three target variables simultaneously, reflecting different aspects of the structure's behaviour, abovementioned (root mean squared error (RMSE) of the model is depicted in Figure S2a).

In addition to these models, another DNN was developed to learn the force-stroke curve of the structure. Given the complexity of this curve, a more complex architecture was employed, with hidden layers comprising 128, 256, and 512 neurons. Before feeding the stiffness curve to the model, it was pre-processed by down sampling to 100 points, simplifying the learning process for the DNN. The down-sampling was executed uniformly and adaptively. The resampling error indicated that the adaptive model had a lower average error (0.28), compared to the uniform method (0.71). Consequently, the adaptive method was chosen, and each stiffness curve was represented by 100 adaptive samples. Each point consisted of x and y values, and as the sampling was adaptive, each curve had different x-values that needed to be accounted for. Two separate DNNs with the same architecture were employed—one to learn the x-values and the other for the y-values (the RMSE error of the model is depicted in Figure S2b).

To ensure model reliability, the dataset was split into training and validation sets using k-fold cross-validation. This technique divides the dataset into five subsets, allowing the network to be trained on a comprehensive set of samples while also evaluating its generalization on unseen data. The cross-validation process offered insights into how well the DNN models generalized across different configurations of the mechanical structure, helping to minimize overfitting and enhance prediction robustness. The training was performed using the Adam optimization algorithm, which is particularly effective for this type of regression task due to its ability to handle sparse gradients and adapt learning rates. The network was trained over 100 epochs, and its progress was continuously monitored to ensure convergence. Performance was primarily assessed using RMSE across each fold, providing a clear measure of the accuracy of the DNN's predictions. The RMSE values for predicting tremor amplitudes required snap-through energy, and maximum snap-through force are 0.36, 1.14, and 0.72 across all folds with percentage errors of 17.9 %, 13.9 % and 4.7 %., respectively. Additionally, the RMSE for models trained on the stiffness curve was 0.02 for x-values and 0.4 for y-values. Fig. S3 shows ten random samples of the DNN output compared to the Simscape results. Additionally, Table S1 represents joint stiffness and the joint angle for these samples.

2.4. Inverse design

The trained DNN model was utilized for the inverse design of the compliant bistable mechanism by integrating it with a GA optimization process. The goal of the inverse design was to find optimal parameter configurations that would allow the bistable mechanism to produce a stiffness curve as close as possible to a predefined desired curve, which consisted of 100 points (the same size as the training data). This process, illustrated in Fig. 4, was essential for customizing the mechanical behaviour of the structure to meet specific design requirements, such as achieving a particular response under varying forces. The optimization began by defining a set of potential parameter configurations. Each configuration represented key attributes of the bistable mechanism, including cross-sectional dimensions, link lengths, angles, and material properties like Young's modulus. An initial population of parameters was generated, and each set was passed through the DNN to predict the resulting stiffness curve.

The GA evaluated the fitness of each parameter configuration by comparing the predicted stiffness curve (obtained via the DNN model) with the desired stiffness curve. The fitness score was calculated using a distance metric, which effectively measured the difference between the desired and predicted curves. In this case, the sum of squared differences was used (the Euclidean distance between each point from the true curve and predicted curve), ensuring that the optimization minimized the total deviation between the two curves. The DNN models played a critical role by providing quick and accurate predictions of stiffness curves, thereby significantly reducing the computational cost of the optimization process. This allowed the GA to perform more iterations and refine the design more efficiently than would have been possible if each evaluation required a full simulation. To validate the effectiveness of the inverse design process, the optimized parameters were used to simulate the structure's behaviour, confirming that the simulation response closely matched the expected results. This validation step ensured that the optimization successfully translated into practical, physical configurations that adhered to the desired mechanical characteristics (Fig. 5).

2.5. Series combination of bistable units

In this research, experimental tests were conducted on a series of compliant bistable units connected in a series configuration. The inverse design was based on properties that were approximated using the superposition theory (instead of simulation of a series of compliant bistable units) to reduce simulation computational costs, based on the simulation and experimental results of just one single bistable unit. Given that these units exhibit nonlinear stiffness characteristics, the validity of the superposition theory needed to be rigorously evaluated in this context. To validate the superposition assumption for multi-unit configurations, 200 simulations of a series configuration consisting of four bistable units were performed (illustrated at Fig. S1). Key parameters, including vibration attenuation (Y), maximum force (X), and required energy (Z) for stretching or compressing the structure, were measured and compared with their approximations $((Y_p), (X_p),$ and $(Z_p))$ derived using the superposition assumption from single-unit simulations.

For vibration attenuation, statistical metrics indicated a strong agreement between the measured Y and approximated Y_p values. Specifically, RMSE was 0.03, and the mean absolute percentage error (MAPE) was 0.18 %. Visualization of Y_p versus Y plots (Fig. 6a) demonstrated strong alignment along the x = y line, while the Bland-Altman plot (Fig. 6b) and distribution approximations (Fig. 6c) confirmed minimal bias and a high degree of correspondence. These results validate the superposition assumption for accurately approximating vibration attenuation in the series configuration.

However, for maximum force X and required energy Z, slight discrepancies were observed between the measured (X, Z) and approximated (X_p, Z_p) values. To address these differences, empirical correction factors (α_X and α_Z) were derived based on the simulation data to minimize the discrepancies. The correction factors, calculated as ($\alpha_X = 1.26$) for maximum force and ($\alpha_Z = 1.10$) for required energy, were applied to adjust the approximations. This approach reduced the RMSE to 7.41 and 3.65 for (X) and (Z), respectively. Correspondingly, the MAPE was

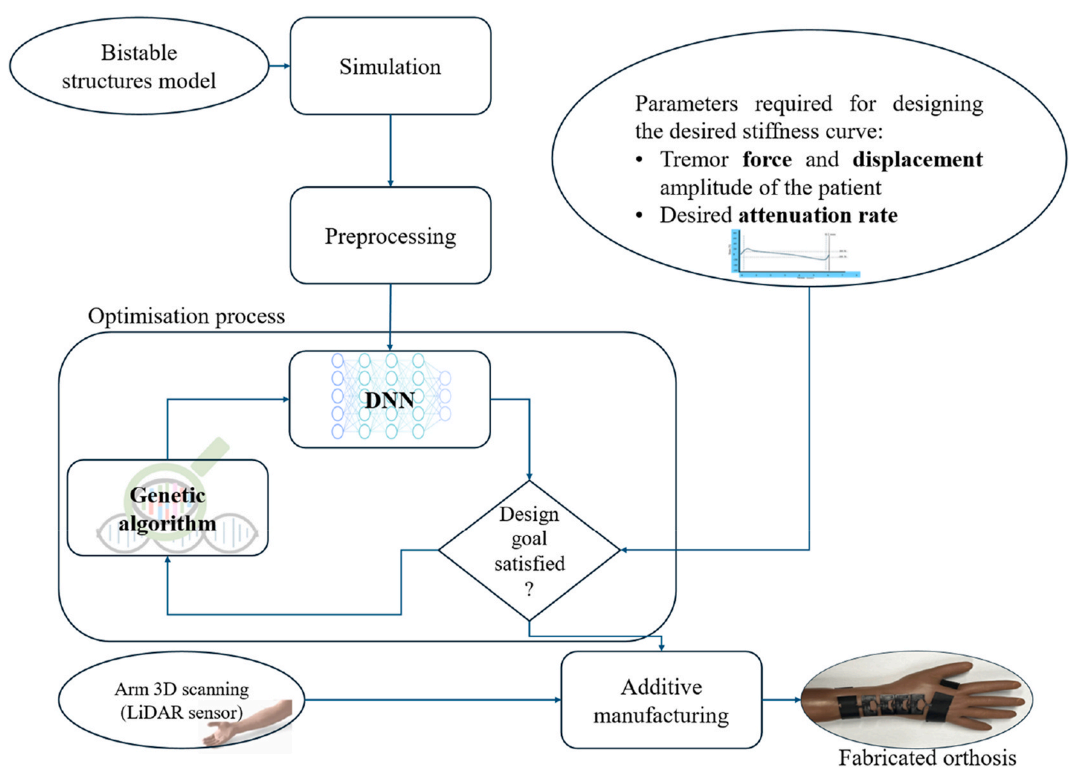

Fig. 4. Inverse design of compliant bistable mechanism for fabricating customised orthosis. The designed orthosis is tested on artificial human arm.

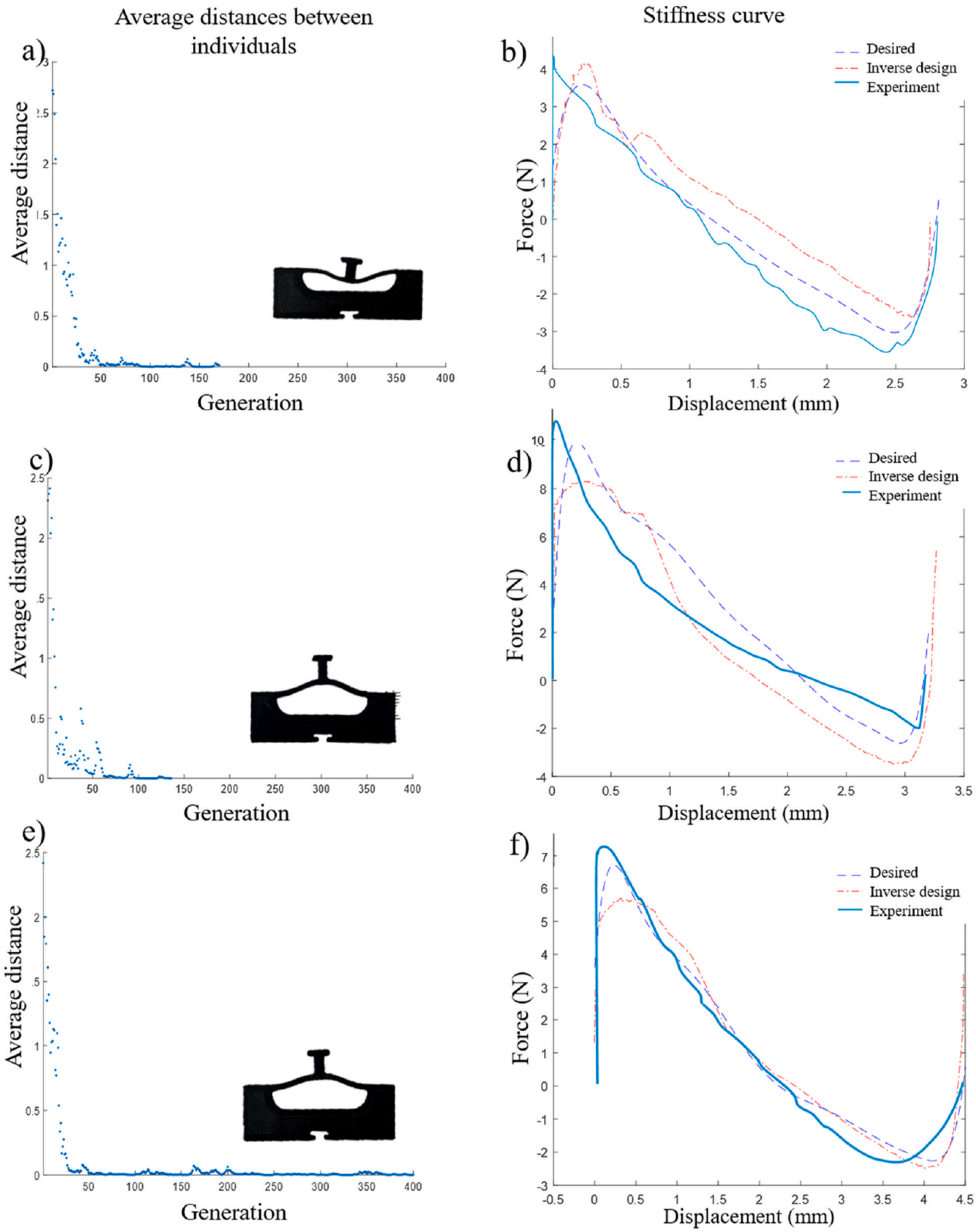

Fig. 5. Three sample inverse designed bistable mechanism units. Average distance between individuals in the GA optimization process for a) sample 01, b) sample 02, and c) sample 03. The stiffness test of the printed sample compared to inverse designed (DNN) output and the desired stiffness curve for a) sample 01, b) sample 02, and c) sample 03.

reduced to 17.96 % for (X) and 10.91 % for (Z). Improved alignment along the x = y line was observed for maximum force (X) and required energy (Z), as shown in Fig. 6d and 6g, respectively. Fig. 6e and 6f illustrate the reduction in errors for maximum force through Bland-Altman and distribution approximations plots, while Fig. 6h and 6i depict similar improvements for required energy. The integration of these correction factors ensures accurate approximations of maximum force and required energy in multi-unit configurations, enhancing the reliability of the design framework while maintaining computational efficiency. These findings underscore the robustness of the proposed superposition-based design methodology for compliant bistable structures. These factors are solely for stiffness tests and not applied in

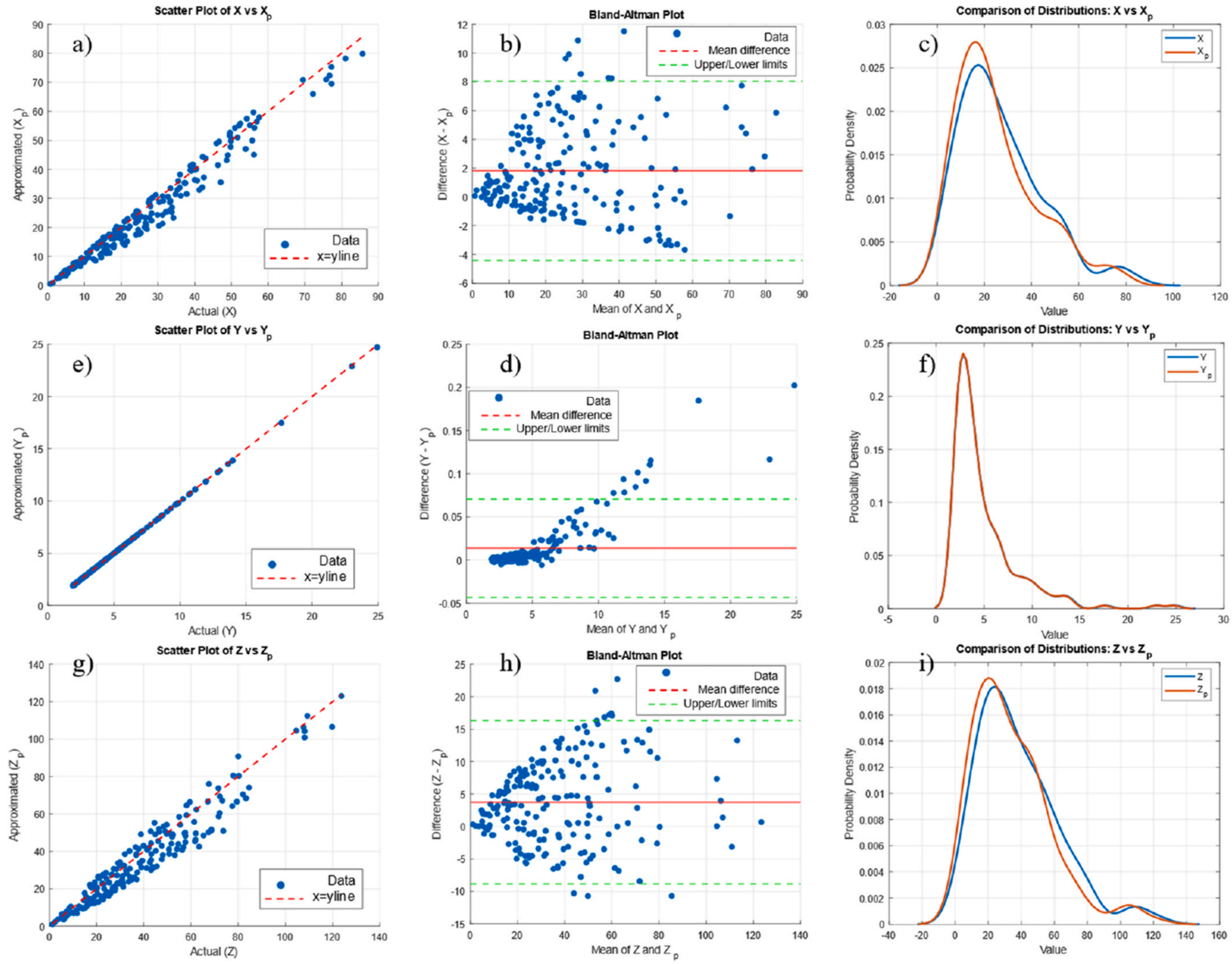

Fig. 6. Comparison of simulation results for a stack of bistable units in a linear configuration with single-unit simulations; then, parameter calculations for the stack based on the superposition. a) Scatter plots of X and X_p, b) Bland Altman plot of X and X_p, and c) probability density of X and X_p. d) Scatter plots of Y and Y_p, e) Bland Altman plot of Y and Y_p, and f) probability density of Y and Y_p. g) Scatter plots of Z and Z_p, h) Bland Altman plot of Z and Z_p, and i) probability density of Z and Z_p.

vibration tests and do not affect the dynamic response of the system in this application as the dynamic test are hold where the units are in the stable states. As such, their inclusion does not hinder the generalizability of the model across different frequencies and amplitudes.

2.6. Experimental procedure

The experimental procedure consists of two main phases: fabrication of the compliant bistable mechanism and experimental testing for stiffness and vibration attenuation. The fabrication phase ensures that the bistable mechanism is accurately produced, whereas the controlled experimental tests confirm its mechanical performance. The stiffness tests evaluate the force-displacement response of the mechanism, while the vibration attenuation tests analyse its effectiveness in mitigating tremor-like oscillations. The following sections provide a detailed description of each phase.

I. Fabrication of the Compliant Bistable Mechanism

The accuracy of the inverse design method was assessed by fabricating a compliant bistable mechanism utilizing ABS plastic. First, Fusion 360 was used to convert the GA optimization's optimal parameters into a comprehensive 3D model. Cura slicing software was then used to prepare the model for 3D printing. Slicing parameters were carefully changed to account for the characteristics of ABS plastic and guarantee structural integrity and layer adhesion.

The 3D printing procedure completed using a Flashforge Guider IIs 3D printer. To reduce defects and enhance mechanical attributes, the following guidelines were set up: 1.75 mm for the filament diameter, 40 mm/s for printing, 35 mm/s for retraction, 230 °C for the nozzle, and 100 °C for the heated bed. In order to reduce frequent printing defects like warping, stringing, and layer misalignment and enhance dimensional accuracy and dependable mechanical performance in the generated samples, these parameters were chosen.

II. Stiffness and Vibration Tests

To assess both the stiffness characteristics and vibration attenuation capabilities of the bistable mechanism, two sets of experiments were conducted.

a) *Force-displacement (stiffness) test* that includes A) The force-displacement response of the mechanism was evaluated using a tensile testing machine (Fig. 7b). B) Measuring the maximum force

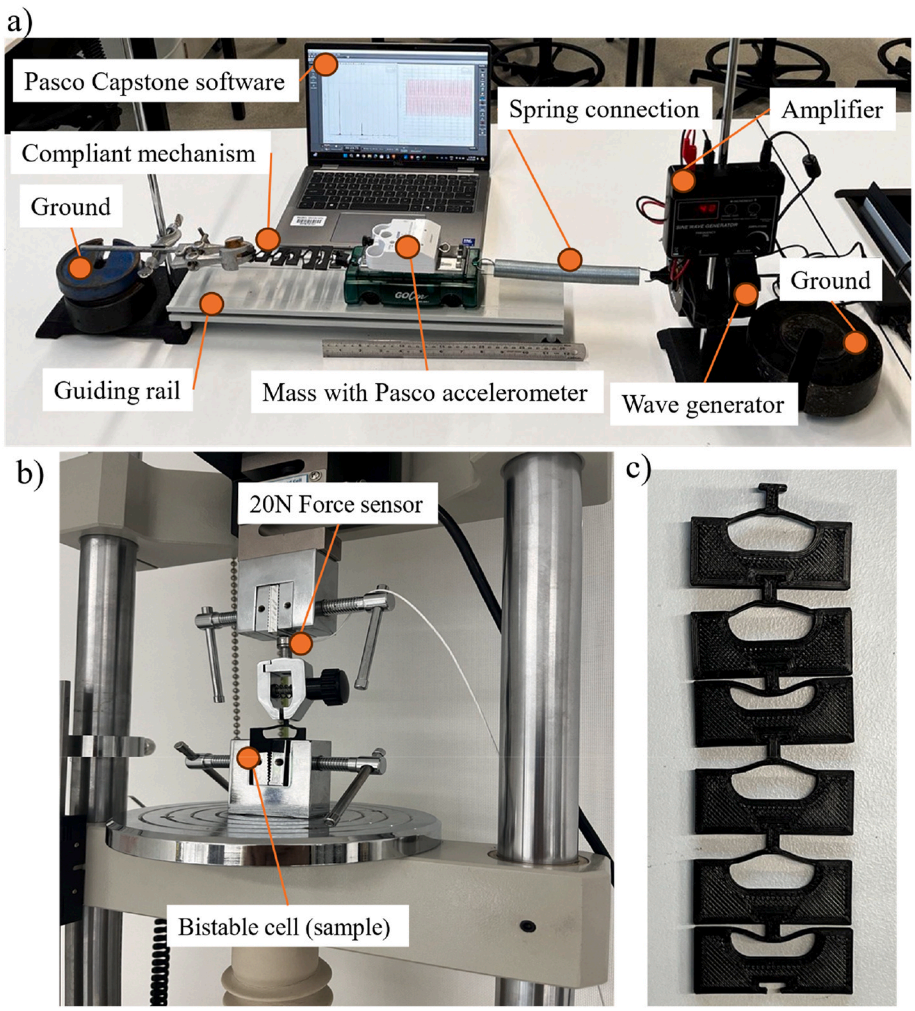

Fig. 7. a) The setup for the vibration attenuation performance of the compliant mechanism. b) The tensile test machine to evaluate the force-displacement curve of the fabricated samples. c) The stack of six bistable units in a series configuration in their first or second stable states.

and energy needed for snap-through and comparing the results with stiffness curves produced by the inverse design method and DNN-based forecasts were the objectives and C) The accuracy of the design and optimization approach was validated by this comparison (Fig. 5).

b) *Vibration attenuation tests* which comprise A) a dynamic experimental setup was designed to replicate tremor-like conditions using a Pasco cart system connected to a signal generator via a spring, with the other end of the generator fixed to the ground (Fig. 7a). B) The signal generator produced sinusoidal waves at different frequencies to simulate tremor conditions. C) The mechanism was installed between the mass (representing a hand) and the ground (representing the forearm in a flexion-extension motion). D) Six parameters were varied to assess the mechanism's effectiveness: 1-Number of bistable units in series (4, 7, or 10) to analyse the impact of multiple units. 2-Hand mass variation (475 g vs. 725 g) to simulate different tremor severity scenarios. 3-Vibration frequency (4 Hz, 5 Hz, 6 Hz) representing typical Parkinson's tremor frequencies. 4-Spring stiffness variation to evaluate different joint stiffness conditions (Figure S4a). 5-Mechanism efficiency is tested on various tremor severity by changing the power in the vibration by keep the amplitude of vibration the same but change the mass of the cart and changing the spring stiffness. 6-Stable-state configurations are changed as shown in Fig. 7c to compare the mechanism's performance across different equilibrium states, and E) these tests were repeated for multiple parameter combinations, and vibration data was collected using a Pasco acceleration sensor at a 100 Hz sampling rate, processed through Pasco Capstone software.

3. Results and discussions

Stiffness and vibration attenuation experiments were performed under various situations to confirm the bistable mechanism's functionality. The force-displacement response of the manufactured samples was measured with a tensile testing machine, and its efficacy in mitigating tremors was examined utilizing a dynamic vibration setup. The number of bistable units, hand mass, vibration frequency, joint stiffness, and stable-state situations were all changed in the various configurations that were examined. A thorough assessment of the mechanism's effectiveness was provided by comparing the outcomes with DNN-based estimations and inverse design predictions.

In the first test, various numbers of the bistable units are attached in a series configuration to evaluate the vibration attenuation of the structure. The structure behaviour can be approximated by supper position theory and spring in series configuration. In this situation, less attenuation is expected, when more bistable units are attached as it results in less stiffness. However, the results showed a significant reduction in vibration amplitude when the compliant mechanism was introduced compared to the baseline scenario without the mechanism. Fig. 8a shows the results in time when the generator frequency is set to 4 Hz. The four-unit mechanism attenuated the vibration more than the other two, while the mechanism with ten units had the lowest

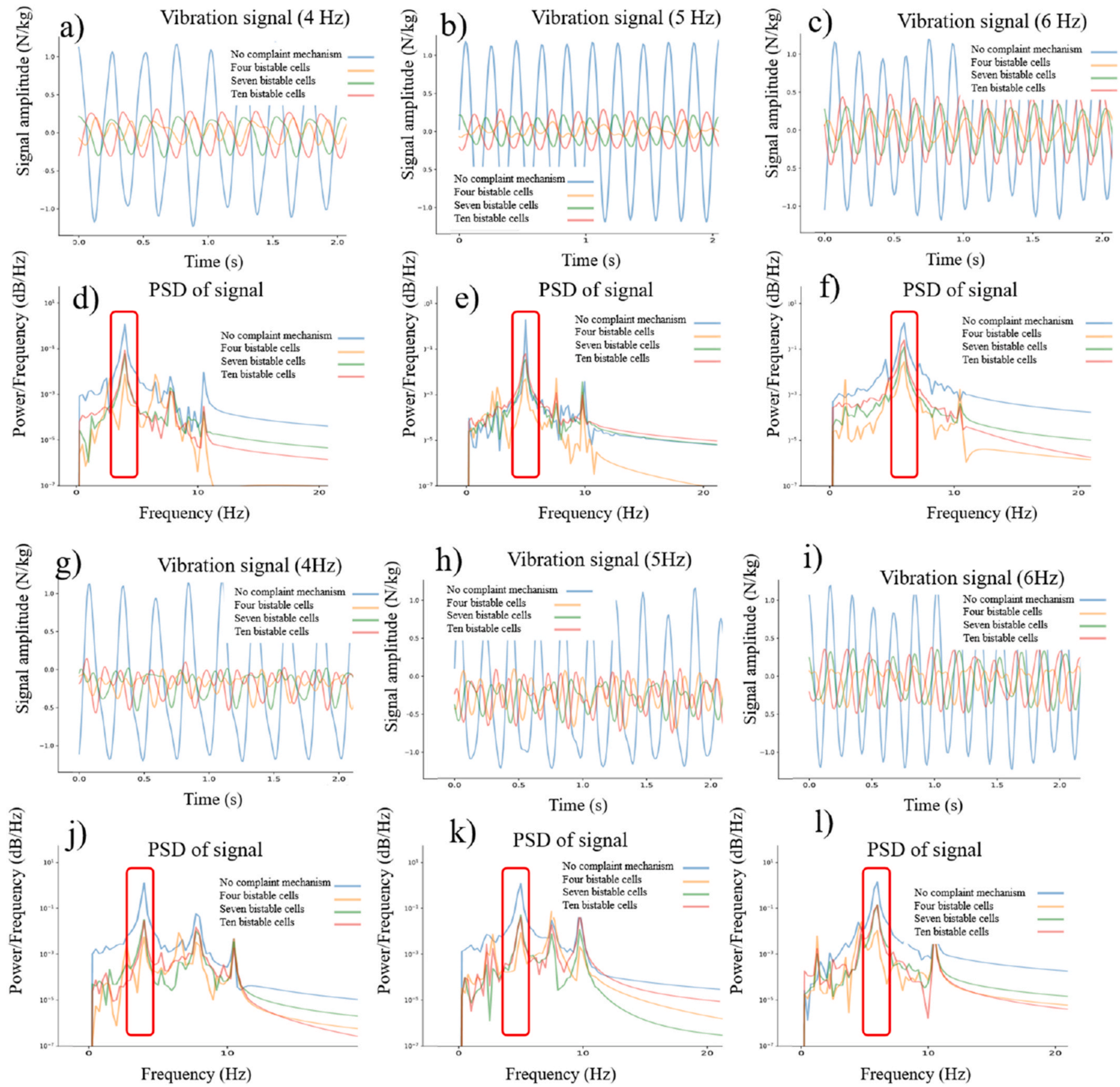

Fig. 8. Experimental results of the vibration attenuation in the compliant bistable mechanism in various scenarios. The setup with higher stiffness spring (30 N/m) vibration signal in time with a) 4 Hz, b) 5 Hz, c) 6 Hz and its power spectrum d) 4 Hz, e) 5 Hz, f) 6 Hz frequency of baseline scenario compared to four, seven and ten bistable units attached to the setup. The vibration signal in time with g) 4 Hz, h) 5 Hz, l) 6 Hz and its power spectrum density (PSD) at i) 4 Hz, j) 5 Hz, k) 6 Hz frequency comparison of the various scenarios for lower stiffness spring setup (8 N/m). The main frequency of the tremor is marked by the red square in the spectrum plots. (For interpretation of the references to colour in this figure legend, the reader is referred to the Web version of this article.)

performance among them.

Fig. 8d shows the power (dB/Hz) of the same set of signals in the frequency domain. The plot shows while all the signals have a peak at 4Hz the power of the vibration is dropped significantly when the compliant mechanism is attached to the setup. Fig. 8b, Fig. 8c, Fig. 8e and Fig. 8 f show the vibration signal in time and frequency for the same set of setups while the signal generator frequency is set to 5 and 6Hz, respectively. This test is repeated to assess the performance of the proposed mechanism in various common frequencies related to PD disease. As it is seen in Fig. 8, the power of the vibration affected by the various lengths of mechanisms is dropped significantly for 5Hz (Fig. 8e) and 6 Hz (Fig. 8f). To evaluate the mechanism effect and performance on the setup is not dependent on the connecting spring's stiffness, another test was conducted with the same length of the mechanism and in the same frequencies. In this set of experiments, the effect of the mechanism was evaluated to see the mechanism performance as a wearable device on different people as the stiffness of the wrist (represented by the connecting spring in the setup) can be different from object to object. The results are depicted in Fig. 8g to Fig. 8i. The peak-to-peak vibration attenuation rate and power mitigation rate at the input frequency for all of the experiments in Fig. 8 are listed in Table S2 and Table S3 in the supplementary document.

More experiments are conducted to explore the characteristics of the mechanism. In another test, the mass in the cart in the setup is changed to model the wrist tremor with a free hand and holding an object (with a mass of 250 g) and assess the mechanism performance in these various situations. This test represents various severity of the tremor as well. Since the applied vibration amplitude remained constant, the larger mass resulted in higher vibration power, effectively modelling more severe tremor conditions. In this test, the free hand mass is 475 as an average adult hand mass and the hand with an extra object weight 725 g. The compliant mechanism includes 4 units, and the excitation signal frequency is 5Hz. The result of the experiment is shown in Fig. 9. The peak-to-peak ratio and the power ratio of the measured vibration before and after the bistable mechanism are stated in Table S4 of the supplementary document. As shown in the Table and the Figure, the attenuation is significant, still in the bigger mass scenario, the vibration peak-to-peak ratio is 3 % more than in the free hand scenario that happens because of the higher mass, there is higher momentum in the system that makes it harder to control the vibration.

Fig. 5 shows that the stiffness of the mechanism in the two stable states is not the same necessarily. Therefore, it is important to explore the mechanisms' vibration mitigation in both stable states. To test the mechanism, various bistable units (samples 01, 02, and 03 in Fig. 5) are printed. The bistable structures include 6 units that are attached in a series configuration, and they are randomly set to the first stable state or second stable state (states are depicted in Fig. 2). The first and second stable states are shown in the experiment as 1 and 0, respectively, and when an experiment is marked as 011011 (this configuration is depicted in Fig. 7b), it means that the units number 2,3,5 and 6 are in state 1 and the 1st and 4th units are in state 0. The results of the experiments are depicted in Fig. S5 in supplementary document and their attenuation ratio is recorded in Table S5, both for peak to peak and signals power attenuation. Results show that in all the combinations, the vibration power is dropped significantly. It can be seen that as some of the samples have less stiffness in state 0, it causes less attenuation in the vibration.

3.1. Tremor attenuation test

A synthetic human arm model was used in a new setup to further explore the potential applications of the designed mechanism (Fig. 10a). The arm was 3D scanned using the Kiri Engine app with the iPhone 15 pro LiDAR sensor, allowing for the customization of the 3D-printed bistable units to fit the arm precisely. Custom fastening bands and bistable units (sample 01 and sample 02 in Fig. 5 with customized bending to fit the synthetic human arm model's wrist) are designed and printed, and the tests were repeated on these new samples to verify the design's performance on attenuating the vibration. The vibration test setup was modified to evaluate the mechanism when mounted on the synthetic human arm model, secured with the fastening bands. The tests were conducted at a frequency of 4 Hz, which is common in PD patients, and the vibration signals were recorded using MetaMotionRL acceleration sensors. The sensor mounted on the arm is aligned with the motion along the Z-axis (perpendicular to the palm), with a recording frequency

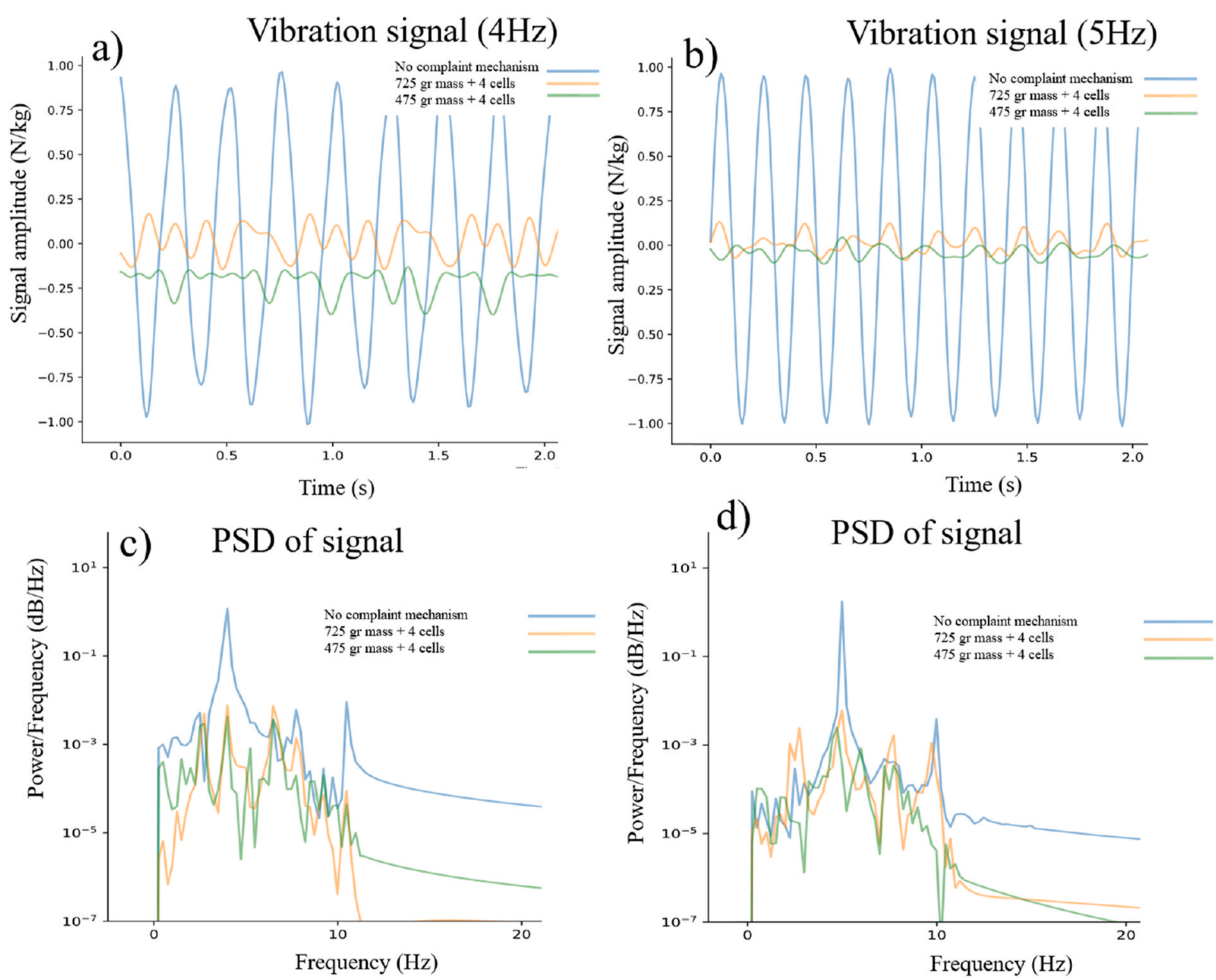

Fig. 9. Experimental results of the vibration attenuation in the compliant bistable mechanism in various scenarios. The setup with two different masses in the cart representing hand and holding object. Vibration signal comparison in time a) for excitation frequency of 4Hz and b) for 5Hz vibration signal and c) PSD of the 4Hz signal and d) 5Hz.

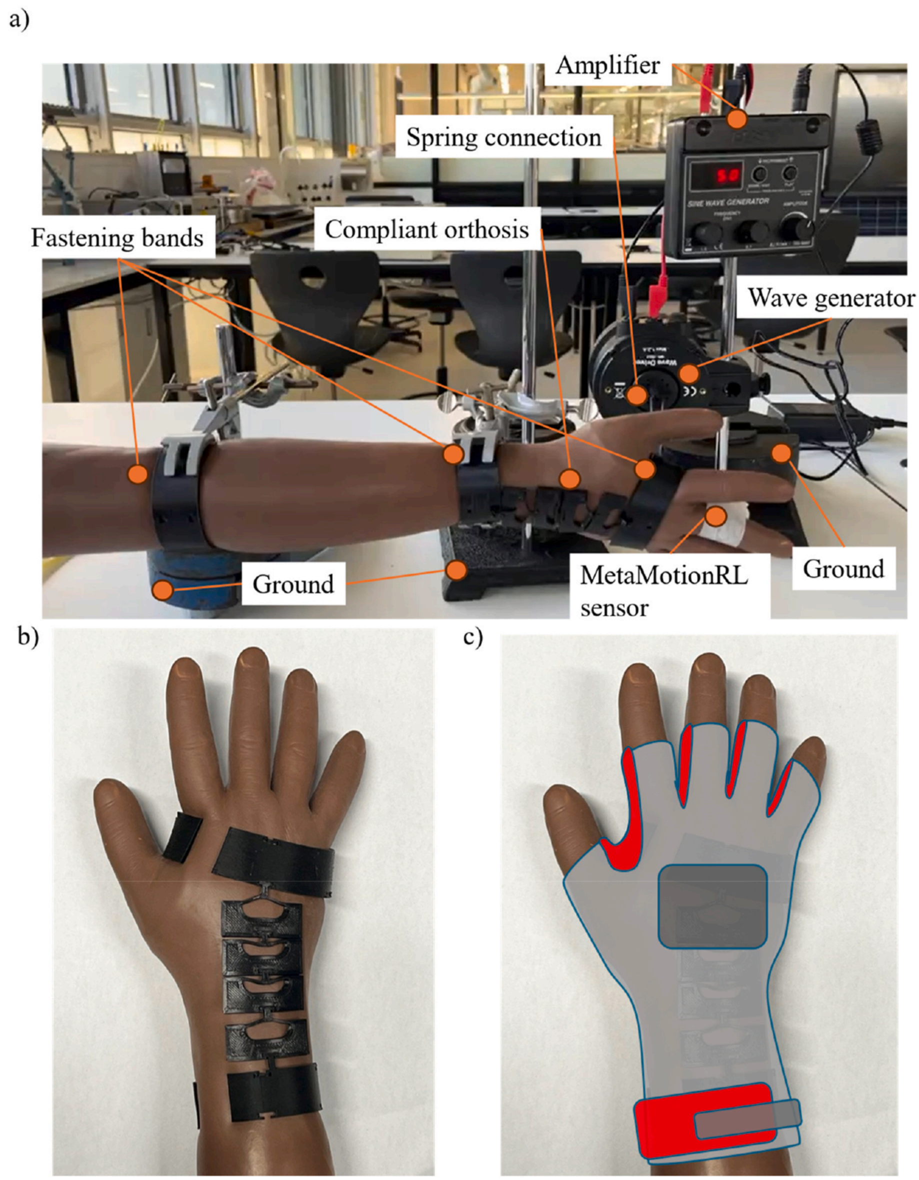

Fig. 10. a) The setup for the vibration attenuation performance of the compliant mechanism on the synthetic human arm model. b) compliant bistable mechanism stack mounted on the arm and c) tremor attenuation wearable glove with an integrated compliant mechanism.

of 100 Hz.

As shown in Fig. 11, the results revealed a significant decrease in tremor amplitude when the orthosis, based on the compliant bistable structure, was attached to the arm. The compliant mechanism mounted on the arm includes four bistable mechanisms. In various scenarios, a mix of samples 01 and 02 are utilized in the orthosis in various stable states (0 or 1) to assess their vibration attenuation. This test is essential, because of the different stiffness of the units in two various states. Additionally, it's important to evaluate the mechanisms' performance in both states, as during extension/flexion of objects wrist, the units can be in any states. The list of the scenarios is listed in Table 1 as well as peak-to-peak attenuation and signals power around 4Hz ratios for the vibration, which reveals that the orthosis can attenuate the power of the tremor up to 87.11 %. To further illustrate the practical benefits of the orthosis, a spoon filled with small metal spheres was attached to the hand, simulating a daily task such as eating. The video results (Videos S1 to S4 in the supplementary document) demonstrate that, without the orthosis, approximately 66 % of the spheres fell from the spoon, whereas none were lost when the orthosis was attached. This indicates the orthosis's potential to assist in daily activities by minimizing involuntary movements. Researchers have integrated various tremor mitigation mechanism in wearable glove for the comfort use of the subjects (Chen et al., 2024; Zhou et al., 2018). In this research, the orthosis can be integrated into a wearable glove which results in a light (just 27 g for bands and 10 bistable units) and flexible tremor mitigator and provides the required comfort for the patient (Fig. 10b and Fig. 10c).

4. Discussions

The efficiency of the proposed bistable structure for tremor reduction was confirmed by the experimental results; yet there were some differences between the simulation and experimental results. Particularly, the limits of the PRBM employed in the simulations and the frequent snap-through-induced deformation of the ABS plastic linkages provide the reason for variances in the stiffness curves. Despite being selected due of its high strength-to-modulus ratio, ABS can undergo minor form changes over time, changing its rigidity properties. Slight differences in structural performance are also caused by dimensional errors that are a natural part of 3D printing. Further developments may look into the usage of more flexible materials, such as thermoplastic polyurethane

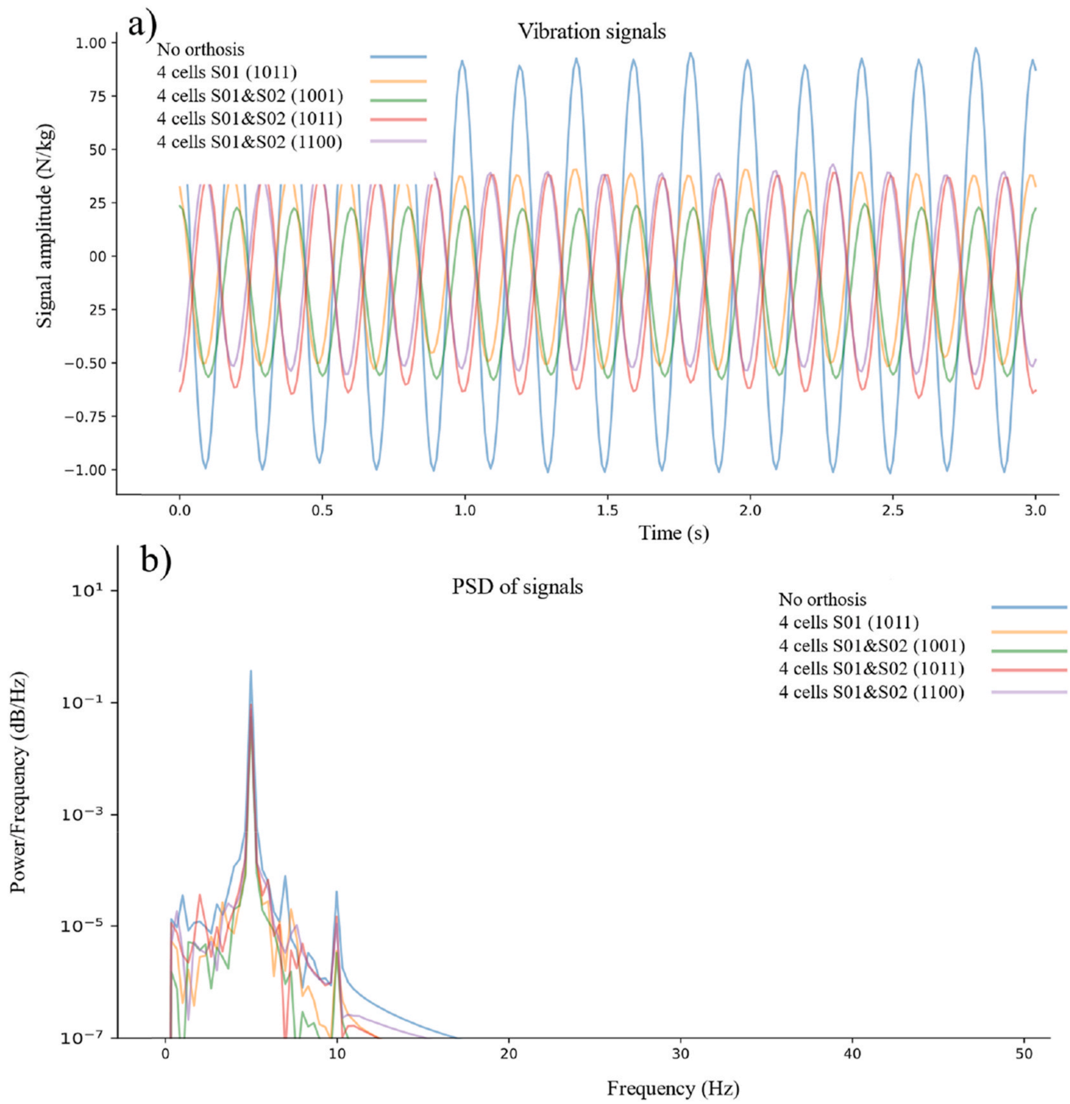

Fig. 11. Experimental results of the vibration attenuation a) in time, and b) the signals PSD in the compliant bistable mechanism on the synthetic human arm model in various scenarios.

Table 1
Peak-to-peak and power ratio percentage of the vibration signal after adding the compliant structure to the synthetic human arm model compared to free vibration.

Experiment	Peak to peak (%)	Power (%)
No orthosis (reference signal)	100 %	100 %
4 units S01 (1011)	41.11 %	16.89 %
4 units S01&S02 (1001)	46.92 %	22.09 %
4 units S01&S02 (1011)	52.09 %	27.37 %
4 units S01&S02 (1100)	48.07 %	23.20 %

(TPU), to reduce such discrepancies and enhance long-term endurance.

Small spaces between the bistable units (connection points) that permitted unwanted movements and marginally decreased the overall attenuation efficiency were another source of inconsistency in the vibration attenuation results. Additionally, the soft substance of the artificial human arm model utilized in the experiments added flexibility, which caused more noticeable vibrations than expected. Refining the design will require addressing these constraints with better fastening methods and increased structural rigidity.

The durability and failure susceptibility of the 3D-printed bistable mechanism were thoroughly examined through material selection, structural optimization, and experimental validation. ABS was selected due to its ability to undergo significant deflection before failure, while design refinements, including increased infill percentage and the addition of wall holders, improved structural rigidity. The primary failure modes identified were beam fractures and wall bending under vibration force. Long-term bistability and resistance to mechanical fatigue remains a critical area for future refinement, by choosing different material and refining the design.

There are various benefits to the suggested wearable device. Being a passive mechanism, it runs without the need for a power source, which makes it sustainable and energy-efficient. This architecture responds instantly to tremor fluctuations because it operates in real-time without signal processing delays, in contrast to active systems that need controllers and actuators. Its adaptability and lightweight design also improve user comfort and usability. The integration of the orthosis into a wearable glove (as illustrated in Fig. 10) provides convenience, and the effective vibration attenuation demonstrated in testing emphasizes the design's feasibility. Additionally, the displacement attained by the orthosis is shown in Fig. 1, demonstrating its versatility and practical advantages.

But there are some restrictions. The snapping force threshold needs to be carefully calibrated since the resistance force produced by the bistable mechanism may obstruct voluntary motion. Moreover, the bistable mechanism's quantized motion limits continuous movement by making it challenging to keep the hand in an unstable posture. Although the flexion/extension wrist motion is the subject of this study, wearable devices for other upper-limb movements, such as protonation/supination or elbow flexion/extension, can be designed using the same methodology. The use of a fabric with low stiffness is crucial when incorporating the mechanism into a wearable glove because it permits smooth transitions between stable states without limiting mobility. The compliant mechanism is attached to firm straps at both ends (to wrap around subject's wrist and palm) to avoid unwanted movement while it provides the comfort for the subject.

The effectiveness of the proposed tremor attenuation mechanism can be contextualized through comparisons with existing passive systems. Prior research in 2018 has shown 85 % efficacy (Buki et al., 2018) in forearm protonation/supination and 80 % efficacy (Rudraraju and Nguyen, 2018b) in elbow tremor reduction. While particle dampers (2020) only reached 37 % efficiency (Lu and Huang, 2021), other passive damping techniques, including the air dashpot (2011) (Takanokura et al., 2011) and airbag damper (2020) (Fromme et al., 2020/04), recorded efficiencies of 82 % and 84 %, respectively. In comparison to several current methods, the suggested bistable mechanism demonstrated higher effectiveness, with tremor power reduction rates of up to 87.11 %. Furthermore, compared to conventional dampers that depend on complicated control systems or external power sources, its passive design and real-time reaction offer clear advantages.

Further modifications could concentrate on improving the design to facilitate smoother voluntary motion by integrating smaller displacement units grouped in sequence in order to further improve usability. Additionally, minimizing differences between simulated and experimental outcomes can be achieved by improving manufacturing accuracy and material selection. This approach may have a wider impact if it is extended to other upper-limb movements, providing a flexible way to treat tremor in a variety of joints. Future research will examine how the bistable mechanism behaves in situations involving both voluntary movement and tremor. This will further validate the mechanism's stability and efficacy in practical applications by examining possible tremor that may occur during voluntary motions.

5. Conclusion

This study presents a compliant bistable mechanism for tremor mitigation, utilizing a unified simulation environment for simulation and inverse design. The mechanism's non-linear stiffness response enables effective vibration attenuation across varying configurations, addressing different user-specific tremor conditions. Through extensive simulations and physical trials, including evaluations on a synthetic human arm model, the model's impact on reducing tremor amplitudes is substantiated, particularly for frequencies commonly associated with Parkinson's disease (4 Hz, 5 Hz, and 6 Hz).

Important experiments evaluated the mechanism's performance by varying a number of parameters, including the stiffness of the connecting spring (which models wrist joint stiffness), vibration frequencies, the mass variations of the vibrating object (475 g for an empty hand model and 725 g for holding an object), and the number of bistable units in series (4, 7, or 10 units). With a notable decrease in vibration amplitude seen for every configuration, these scenarios demonstrated the design's adaptability to various application cases. For instance, the configuration with four units demonstrated higher attenuation performance at 4 Hz compared to the seven- and ten-unit setups, likely due to increased stiffness in shorter mechanisms. At higher frequencies, such as 5 Hz and 6 Hz, similar trends were observed, with performance generally decreasing as more units were added. Power of vibration attenuation rates across configurations in these tests reached 92.64 % (4 Hz), 95.47 % (5 Hz), and 81.22 % (6 Hz) in the worst-case scenario. Additionally, the mechanism's resilience across user-specific wrist stiffness conditions was further validated by adjusting the connecting spring stiffness.

Additionally, tests comparing different hand masses provided insights into the mechanism's adaptability to variable load conditions, with amplitude attenuation rates of 87.72 % for the 475 g hand and 84.77 % for the 725 g hand. These results indicate that, although heavier loads slightly decrease control over vibration due to increased momentum, the mechanism effectively dampens tremor across both conditions. Finally, tests examining the bistable units' behaviour across stable states showed that the configuration of units in either stable state significantly impacts stiffness.

The successful integration of DNN models and genetic algorithms facilitated rapid prediction and optimization of the mechanism's configurations, supporting tailored designs with specific stiffness properties. Further the demonstrating the resilience of this technique is experimental validation using 3D-printed models, that is executed by 3D scanning a synthetic human arm model to customize the proposed bistable structure, that closely resemble the expected behaviour while the whole structure weigh just 27 g. By showcasing a modifiable, compliant mechanism that can be incorporated into a wearable orthotic, like a glove, this study advances tremor mitigation technology and helps patients with tremor-related diseases. To optimize comfort and efficacy, future directions include expanding trials across a variety of patient scenarios and improving material choices towards 4D printing. With promising impacts for wearable technology aimed at treating upper limb tremors in humans, this work highlights the potential of compliant bistable systems for therapeutic applications.

CRediT authorship contribution statement

Moslem Mohammadi: Writing – review & editing, Writing – original draft, Visualization, Validation, Methodology, Investigation, Formal analysis, Data curation. **Abbas Z. Kouzani:** Writing – review & editing, Supervision, Methodology, Investigation, Formal analysis. **Mahdi Bodaghi:** Writing – review & editing, Supervision, Methodology, Investigation. **Ali Zolfagharian:** Writing – review & editing, Supervision, Resources, Project administration, Investigation, Funding acquisition, Conceptualization.

6. Compliance with ethics guidelines

This article does not contain any studies with human or animal subjects performed by any of the authors.

Declaration of competing interest

The authors declare that they have no known competing financial interests or personal relationships that could have appeared to influence the work reported in this paper.

Acknowledgments

Ali Zolfagharian acknowledges the support by Australian Research Council under the Discovery Early Career Award [project number DE240100960] funded by the Australian Government. Mahdi Bodaghi acknowledges the support by the UK Engineering and Physical Sciences Research Council (EPSRC) (award no. EP/Y011457/1) and by the RAEng/Leverhulme Trust Research Fellowship (award no. LTRF-2324-20-129).

Appendix A. Supplementary data

Supplementary data to this article can be found online at https://doi.org/10.1016/j.jmbbm.2025.107006.

Data availability

Data will be made available on request.

References

Achleitner, J., Rohde-Brandenburger, K., Rogalla von Bieberstein, P., Sturm, F., Hornung, M., 2019. Aerodynamic design of a morphing wing sailplane. In: AIAA Aviation 2019 Forum, p. 2816.
Armstrong, M.J., Okun, M.S., 2020. Diagnosis and treatment of parkinson disease: a review. JAMA 323 (6), 548–560. https://doi.org/10.1001/jama.2019.22360.
Baizabal-Carvallo, J.F., Kagnoff, M.N., Jimenez-Shahed, J., Fekete, R., Jankovic, J., 2014. The safety and efficacy of thalamic deep brain stimulation in essential tremor: 10 years and beyond. J. Neurol. Neurosurg. Psychiatry 85 (5), 567–572. https://doi.org/10.1136/jnnp-2013-304943.
Bao, G., et al., 2019. Academic review and perspectives on robotic exoskeletons. IEEE Trans. Neural Syst. Rehabil. Eng. 27 (11), 2294–2304.
Bazmara, M., Mianroodi, M., Silani, M., 2023. Application of physics-informed neural networks for nonlinear buckling analysis of beams. Acta Mech. Sin. 39 (6), 422438.
Bilancia, P., Berselli, G., 2021. An overview of procedures and tools for designing nonstandard beam-based compliant mechanisms. Comput. Aided Des. 134, 103001.
Buki, E., Katz, R., Zacksenhouse, M., Schlesinger, I., 2018. Vib-bracelet: a passive absorber for attenuating forearm tremor. Med. Biol. Eng. Comput. 56 (5), 923–930. https://doi.org/10.1007/s11517-017-1742-7.
Chen, S., et al., 2023. Elastic architected mechanical metamaterials with negative stiffness effect for high energy dissipation and low frequency vibration suppression. Compos. B Eng. 267, 111053.
Chen, Y., Li, J., Yang, X., Wang, Y., 2024. Tunable Stiffness Glove for Tremor Suppression Based on 3D Printed Structured Fabrics. 2024 IEEE/RSJ International Conference on Intelligent Robots and Systems (IROS), IEEE, pp. 10543–10549.
Cury, R.G., et al., 2017. Thalamic deep brain stimulation for tremor in Parkinson disease, essential tremor, and dystonia. Neurology 89 (13), 1416–1423. https://doi.org/10.1212/WNL.0000000000004295.
Deng, B., Zareei, A., Ding, X., Weaver, J.C., Rycroft, C.H., Bertoldi, K., 2022. Inverse design of mechanical metamaterials with target nonlinear response via a neural accelerated evolution strategy. Adv. Mater. 34 (41), 2206238.
Fromme, N.P., Camenzind, M., Riener, R., Rossi, R.M., 2020. Design of a lightweight passive orthosis for tremor suppression. J. NeuroEng. Rehabil. 17 (1), 47. https://doi.org/10.1186/s12984-020-00673-7.
Gomez, M., Moulton, D.E., Vella, D., 2017. Critical slowing Down in purely elastic 'snap-through'instabilities. Nat. Phys. 13 (2), 142–145.
Hao, G., Li, H., Nayak, A., Caro, S., 2018. Design of a compliant gripper with multimode jaws. J. Mech. Robot. 10 (3), 031005.
Herrnstadt, G., Menon, C., 2013. "On-Off Tremor Suppression Orthosis with Electromagnetic Brake,". https://doi.org/10.11159/ijmem.2013.002.
Herrnstadt, G., McKeown, M.J., Menon, C., 2019. Controlling a motorized orthosis to follow elbow volitional movement: tests with individuals with pathological tremor. J. NeuroEng. Rehabil. 16 (1), 23. https://doi.org/10.1186/s12984-019-0484-1.
Holst, G.L., Teichert, G.H., Jensen, B.D., 2011. "Modeling and Experiments of Buckling Modes and Deflection of fixed-guided Beams in Compliant Mechanisms,".
Howell, L.L., 2013. Compliant mechanisms. In: 21st Century Kinematics: the 2012 NSF Workshop. Springer, pp. 189–216.
Huang, H.-W., Yang, Y.-J., 2012. A MEMS bistable device with push-on–push-off capability. J. Microelectromech. Syst. 22 (1), 7–9.
Jin, M., Yang, Z., Ynchausti, C., Zhu, B., Zhang, X., Howell, L.L., 2020. Large-deflection analysis of general beams in contact-aided compliant mechanisms using chained pseudo-rigid-body model. J. Mech. Robot. 12 (3), 031005.
Kumar, S., Tan, S., Zheng, L., Kochmann, D.M., 2020. Inverse-designed spinodoid metamaterials. npj Comput. Mater. 6 (1), 73.
Li, S., Hao, G., 2021. Current trends and prospects in compliant continuum robots: a survey. In: Actuators, vol. 10. MDPI, p. 145, 7.
Li, Z., et al., 2023. Network topology optimization via deep reinforcement learning. IEEE Trans. Commun. 71 (5), 2847–2859. https://doi.org/10.1109/TCOMM.2023.3244239.
Librandi, G., Tubaldi, E., Bertoldi, K., 2020. Snapping of hinged arches under displacement control: strength loss and nonreciprocity. Phys. Rev. 101 (5), 053004.
Ling, M., Yuan, L., Luo, Z., Huang, T., Zhang, X., 2022. Enhancing dynamic bandwidth of amplified piezoelectric actuators by a hybrid lever and bridge-type compliant mechanism. In: Actuators, vol. 11. MDPI, p. 134, 5.
Liu, T., Hao, G., 2022. Design of deployable structures by using bistable compliant mechanisms. Micromachines 13 (5), 651.
Liu, F., Jiang, X., Wang, X., Wang, L., 2020. Machine learning-based design and optimization of curved beams for multistable structures and metamaterials. Extreme Mechanics Letters 41, 101002.
Liu, W., Zhang, Y., Lyu, Y., Bosiakov, S., Liu, Y., 2023. Inverse design of anisotropic bone scaffold based on machine learning and regenerative genetic algorithm. Front. Bioeng. Biotechnol. 11.
Liu, T., Hao, G., Zhu, J., Kuresangsai, P., Abdelaziz, S., Wehrle, E., 2024. Modeling compliant bistable mechanisms: an energy method based on the high-order smooth curvature model. Int. J. Mech. Sci. 275, 109315.
Lu, Z., Huang, Z., 2021. Analytical and experimental studies on particle damper used for tremor suppression. J. Vib. Control 0 (0), 1077546320969469. https://doi.org/10.1177/1077546320969469.
Marsden, C.D., 1984. Origins of normal and pathological tremor. In: Findley, L.J., Capildeo, R. (Eds.), Movement Disorders: Tremor. Palgrave Macmillan UK, London, pp. 37–84.
Masoumi, M.M., 2018. Passive Hand Tremor Attenuator: Magnetic Spring. University of British Columbia.
Masters, N.D., Howell, L.L., 2003. A self-retracting fully compliant bistable micromechanism. J. Microelectromech. Syst. 12 (3), 273–280.
McGowan, P., Hao, G., 2023. Design of a morphing compliant mechanism with separate gripping and retraction modes using a single actuation. J. Mech. Robot. 15 (1), 015002.
Milner, T.E., Cloutier, C., 1998. Damping of the wrist joint during voluntary movement. Exp. Brain Res. 122, 309–317.
Mohammadi, M., Zolfagharian, A., Bodaghi, M., Xiang, Y., Kouzani, A.Z., 2022. 4D printing of soft orthoses for tremor suppression. Bio-Design and Manufacturing 5 (4), 786–807.
Mohammadi, M., Kouzani, A.Z., Bodaghi, M., Xiang, Y., Zolfagharian, A., 2023. 3D-Printed phase-change artificial muscles with autonomous vibration control. Advanced Materials Technologies, 2300199.
Mohammadi, M., et al., 2024. Sustainable robotic joints 4D printing with variable stiffness using reinforcement learning. Robot. Comput. Integrated Manuf. 85, 102636.
Nazari, F., Mohajer, N., Nahavandi, D., Khosravi, A., Nahavandi, S., 2023. Applied exoskeleton technology: a comprehensive review of physical and cognitive human–robot interaction. IEEE Transactions on Cognitive and Developmental Systems 15 (3), 1102–1122.
Odhner, L.U., Dollar, A.M., 2012. The smooth curvature model: an efficient representation of euler–bernoulli flexures as robot joints. IEEE Transactions on Robotics 28 (4), 761–772.
Oladipo, B., Matos, H., Krishnan, N.A., Das, S., 2023. Integrating experiments, finite element analysis, and interpretable machine learning to evaluate the auxetic response of 3D printed re-entrant metamaterials. J. Mater. Res. Technol. 25, 1612–1625.
Puschmann, A., Wszolek, Z.K., 2011. Diagnosis and treatment of common forms of tremor. Semin. Neurol. 31 (1), 65–77. https://doi.org/10.1055/s-0031-1271312.
Radisson, B., Kanso, E., 2023. Elastic snap-through instabilities are governed by geometric symmetries. Phys. Rev. Lett. 130 (23), 236102.
Rastegarzadeh, S., Wang, J., Huang, J., 2023. Neural network-assisted design: a study of multiscale topology optimization with smoothly graded cellular structures. J. Mech. Des. 145 (1), 011701.
Rudraraju, S., Nguyen, T., 2018a. Wearable tremor reduction device (TRD) for human hands and arms. In: Frontiers in Biomedical Devices, vol. 40789. American Society of Mechanical Engineers, V001T10A010.
Rudraraju, S., Nguyen, T., 2018b. Wearable tremor reduction device (TRD) for human hands and arms. In: 2018 Design of Medical Devices Conference. 2018 Design of Medical Devices Conference, V001T10A010. https://doi.org/10.1115/dmd2018-6918 [Online]. Available:
Sasso, E., Perucca, E., Fava, R., Calzetti, S., 1990. Primidone in the long-term treatment of essential tremor: a prospective study with computerized quantitative analysis. Clin. Neuropharmacol. 13 (1), 67–76. https://doi.org/10.1097/00002826-199002000-00007.
Sen, S., Awtar, S., 2013. A closed-form nonlinear model for the constraint characteristics of symmetric spatial beams. J. Mech. Des. 135 (3), 031003.
Shanker, V., 2019. Essential tremor: diagnosis and management. BMJ 366, l4485. https://doi.org/10.1136/bmj.l4485.
Skaramagkas, V., Andrikopoulos, G., Manesis, S., 2021. Towards essential hand tremor suppression via pneumatic artificial muscles. Actuators 10 (9). https://doi.org/10.3390/act10090206.
Takanokura, M., Sugahara, R., Miyake, N., Ishiguro, K., Muto, T., Sakamoto, K., 2011. "UPPER-LIMB ORTHOSES IMPLEMENTED WITH AIR DASHPOTS FOR SUPPRESSION OF PATHOLOGICAL TREMOR IN DAILY ACTIVITES,".
Voloshina, A.S., 2024. Robotic Exoskeleton Adapts to Its Wearer Through Simulated Training. Nature Publishing Group UK, London.
Wang, W., Amirkhizi, A.V., 2023. Reduced order modeling of dynamic mechanical metamaterials for analysis of infinite and finite systems. J. Appl. Mech. 90 (9).
Wu, Z., Xu, Q., 2022. Design of a structure-based bistable piezoelectric energy harvester for scavenging vibration energy in gravity direction. Mech. Syst. Signal Process. 162, 108043.
Yang, H., Ma, L., 2019. Multi-stable mechanical metamaterials by elastic buckling instability. J. Mater. Sci. 54 (4), 3509–3526.
Yang, H., Ma, L., 2020. 1D to 3D multi-stable architected materials with zero Poisson's ratio and controllable thermal expansion. Mater. Des. 188, 108430.
Yu, Y.-Q., Zhu, S.-K., 2017. 5R pseudo-rigid-body model for inflection beams in compliant mechanisms. Mech. Mach. Theor. 116, 501–512.
Yu, Y.-Q., Howell, L.L., Lusk, C., Yue, Y., He, M.-G., 2005. "Dynamic Modeling of Compliant Mechanisms Based on the pseudo-rigid-body Model,".
Zahedi, A., Zhang, B., Yi, A., Zhang, D., 2021. A soft exoskeleton for tremor suppression equipped with flexible semiactive actuator. Soft Robot. 8 (4), 432–447. https://doi.org/10.1089/soro.2019.0194 (in eng).
Zeng, Q., Duan, S., Zhao, Z., Wang, P., Lei, H., 2023. Inverse design of energy-absorbing metamaterials by topology optimization. Adv. Sci. 10 (4), 2204977.
Zhang, Z., et al., 2024. Bistable characteristics of deployable carbon fiber/bismaleimide resin composite shells in megathermal environments. Mech. Adv. Mater. Struct. 31 (7), 1633–1644.
Zhang, Z., et al., 2025. Inverse design method of deployable cylindrical composite shells for solar sail structure. Compos. Struct. 352, 118698.

Zheng, X., Zhang, X., Chen, T.T., Watanabe, I., 2023. Deep learning in mechanical metamaterials: from prediction and generation to inverse design. Adv. Mater. 35 (45), 2302530.

Zhou, Y., Jenkins, M.E., Naish, M.D., Trejos, A.L., 2018. Development of a wearable tremor suppression glove. In: 2018 7th IEEE International Conference on Biomedical Robotics and Biomechatronics (Biorob). IEEE, pp. 640–645.

Zirbel, S.A., Tolman, K.A., Trease, B.P., Howell, L.L., 2016. Bistable mechanisms for space applications. PLoS One 11 (12), e0168218.

Zolfagharian, A., Demoly, F., Lakhi, M., Rolfe, B., Bodaghi, M., 2025. Bistable mechanisms 3D printing for mechanically programmable vibration control. Adv. Eng. Mater., 2402233